Macromolecular Symposia Vol. 265

Modern Polymer Spectroscopy

Selected Contributions from the conference:
"17th European Symposium on Polymer Spectroscopy (ESOPS 17)"
Seggauberg, Austria, September 9–12, 2007

Symposium Editor:
Peter Wilhelm
(Graz University of Technology, Austria)

ISBN 3-527-32438-0

WILEY-VCH

Macromolecular Symposia | 265

Modern Polymer Spectroscopy

Selected Contributions from the conference:
"17th European Symposium on Polymer Spectroscopy (ESOPS 17)"
Seggauberg, Austria, September 9–12, 2007

Symposium Editor:
Peter Wilhelm
(Graz University of Technology, Austria)

M. Laus, D. Ferri, P. Lomellini (Eds.)

From Polymer Structure and Rheology to Process Modeling EUPOC 2007

Vol. 263

Th. Heinze, M. Janura, A. Koschella (Eds.)

Structure and Properties of Cellulose

Vol. 262

S. Zhu, B. Li (Eds.)

Advanced Materials and Polymer Reaction Engineering Hangzhou International Polymer Forum

Vol. 261

B. Liu, M. Terano, V. Busico (Eds.)

Heterogeneous Ziegler-Natta Catalysts

Vol. 260

H.-U. Moritz, W. Pauer (Eds.)

Polymer Reaction Engineering - 9th International Workshop

Vol. 259

M. Hess (Ed.)

Polychar-15 World Forum on Advanced Materials

Vol. 258

Macromolecular Symposia Vol. 265

Modern Polymer Spectroscopy

Selected Contributions from the conference:
"17th European Symposium on Polymer Spectroscopy (ESOPS 17)"
Seggauberg, Austria, September 9–12, 2007

Symposium Editor:
Peter Wilhelm
(Graz University of Technology, Austria)

ISBN 3-527-32438-0

WILEY-VCH

Full text and further information: www.ms-journal.de

Macromolecular Symposia
is published 14 times a year

Annual subscription rates 2008
Macromolecular Full Package
(All seven *Macromolecular Journals*; 101 issues in total):

Europe	Euro	8,999	9,899
Switzerland	Sfr	14,995	16,495
All other areas	US$	11,895	13,085
		print only **or** electronic only	print **and** electronic

Postage and handling charges included.
All Wiley-VCH prices are exclusive of VAT.
Prices are subject to change.
Individual subscriptions, single issues and back copies are available.
Please ask for details at: service@wiley-vch.de

Orders may be placed through your bookseller or directly at the publishers:
WILEY-VCH Verlag GmbH & Co. KGaA,
P.O. Box 10 11 61, 69451 Weinheim, Germany,
Tel. +49 (0) 62 01/6 06-400,
Fax +49 (0) 62 01/60 61 84,
E-mail: service@wiley-vch.de

Copyright Permission:
Fax: +49 (0) 62 01/6 06-332,
E-mail: rights@wiley-vch.de

For USA and Canada: Macromolecular Symposia (ISSN 1022-1360) is published with 14 volumes per year by WILEY-VCH Verlag GmbH & Co. KGaA, Boschstr. 12, 69451 Weinheim, Germany. Air freight and mailing in the USA by Publications Expediting Inc., 200 Meacham Ave., Elmont, NY 11003, USA. Application to mail at Periodicals Postage rate is pending at Jamaica, NY 11431, USA. POSTMASTER please send address changes to: Macromolecular Symposia, c/o Wiley-VCH, III River Street, Hoboken, NJ 07030, USA.

Printed on acid-free paper.
Typesetting: Thomson Digital (India) Ltd., India
Printing: Strauss Offsetdruck, Mörlenbach
Binding: Litges & Dopf, Heppenheim

Macromolecular Symposia: Vol. 265

Articles published on the web will appear several weeks before the print edition. They are available through:

WILEY InterScience®

www.interscience.wiley.com

Cover: The 17th European Symposium on Polymer Spectroscopy (ESOPS17) was held on September 9–12, 2007 in Seggauberg, Austria. The biennial series of ESOPS meetings brings together scientists specialized in various spectroscopic methods.

The cover picture, is taken from the contribution by Chernev et al. p. 272 and shows infrared images of multilayer polymer film.

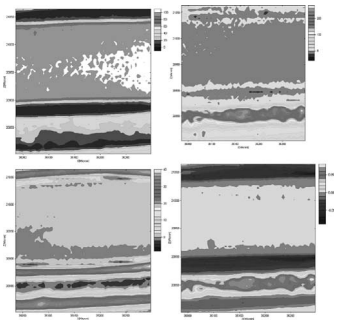

Modern Polymer Spectroscopy

Seggauberg, Austria, September 9–12, 2007

This volume contains selected presentations from the 17th European Symposium on Polymer Spectroscopy (ESOPS17), presented either as invited, short oral or poster contributions. The meeting was organized by the Austrian Centre for Electron Microscopy and Nanoanalysis (formed by the Institute for Electron Microscopy of the Graz University of Technology and the Graz Centre for Electron Microscopy). ESOPS 17 was held from 9th to 12th September 2007 and took place in the ancient castle of Seggauberg, which is situated in the Styrian wine region, near Austria's borders to Slovenia and Hungary.

The biennial series of ESOPS meetings brings together scientists specialized in various spectroscopic methods, from both academic institutions and industry. 103 scientists and students participated in ESOPS17, coming from 27 nations, mainly from Central and Eastern Europe, but also from America (Canada, USA, Venezuela), Africa (Algeria), Asia (India, Japan) and Australia. They discussed the latest developments in the spectroscopic characterization of polymeric materials. Methods, like infrared and Raman spectroscopy and imaging, NMR and ESR spectroscopy, dielectric spectroscopy, also in combination with light and electron microscopy and near-field imaging, were covered by 10 invited lectures, 30 short oral and 45 poster contributions.

Professor Heinz Siesler, member of the International Advisory Board, presented poster awards to Dennis Aulich (ISAS Institute for Analytical Sciences, Berlin), Matt Parkinson (Borealis Polyolefine GmbH, Linz) and Christian Vogel (University of Duisburg-Essen); all three posters dealt with characterisation of polymeric samples by different spectroscopic approaches.

An exhibition of new instrumentation, presented by 10 companies, and new publications on polymer analytics, courtesy of 3 publishers, completed the programme. During the social programme the participants could enjoy local dishes, wine and music, and visit the city of Graz.

The editors would like to thank all the contributors and reviewers, as well as the staff of *Macromolecular Symposia* for their co-operation in preparing this proceedings volume. Additionally, we wish to thank all those who contributed to the success of our symposium, namely the sponsors and the members of the International Advisory Board and the local organising committee.

Peter Wilhelm

Participants from the "17th European Symposium on Polymer Spectroscopy (ESOPS 17)"

Micro-Raman and Tip-Enhanced Raman Spectroscopy of Carbon Allotropes

Günter G. Hoffmann,[*1,2] *Gijsbertus de With,*[1] *Joachim Loos*[*1,3]

Summary: Raman spectroscopic data are obtained on various carbon allotropes like diamond, amorphous carbon, graphite, graphene and single wall carbon nanotubes by micro-Raman spectroscopy, tip-enhanced Raman spectroscopy and tip-enhanced Raman spectroscopy imaging, and the potentials of these techniques for advanced analysis of carbon structures are discussed. Depending on the local organisation of carbon the characteristic Raman bands can be found at different wavenumber positions, and e.g. quality or dimensions of structures of the samples quantitatively can be calculated. In particular tip-enhanced Raman spectroscopy allows the investigation of individual single wall carbon nanotubes and graphene sheets and imaging of e.g. local defects with nanometer lateral resolution. Raman spectra of all carbon allotropes are presented and discussed.

Keywords: carbon allotropes; graphene; raman spectroscopy; single wall carbon nanotubes; TERS

Introduction

Carbon is known to exist in a number of allotropes, which range from the hardest of all known material, the pure and single crystalline diamond, to the soft, mainly amorphous, and very impure carbon in the form of soot or glassy carbon. Three of those, diamond, graphite, and of course soot are known since ancient times, while the monomolecular forms of carbon, carbon nanotubes and the Buckminsterfullerenes have been discovered only some years ago.[1,2] These forms can be classified as three-dimensional (diamond and graphite, Figure 1a and b), one-dimensional (single wall carbon nanotubes, Figure 1d), and zero-dimensional (Buckminsterfullerene, C_{60}, Figure 1e). Only recently, in 2004, Gaim and Novoselov[3] produced the two-dimensional form of carbon, graphene by "simply" removing sheet after sheet from graphite to gain a single graphene layer (Figure 1c); and attention is paid to this form of carbon because of its extraordinary functional properties, and potential low production costs.[4]

Since it is possible to produce the allotropes of carbon in large quantities, making it feasible to use them for numerous applications,[5] it has become more and more important to analyze these materials being able to establish, ultimately, structure-property relations at the nanometer length scale. Raman spectroscopy, and in particular micro-Raman,[6] surface enhanced Raman spectroscopy (SERS)[7] or tip-enhanced Raman spectroscopy (TERS) recently introduced[8,9] are characterisation techniques that are able to provide chemical as well as functional information on these materials.

The latter one, TERS, is a characterisation technique combining the power of Raman spectroscopy to reveal chemical composition and molecular structure with the ultra-high spatial resolution of scanning probe microscopy (SPM). Theoretically, TERS allows spectroscopic analysis of any kind of macromolecular material (as

[1] Eindhoven University of Technology, P.O. Box 513, 5600 MB Eindhoven, The Netherlands
E-mail: g.g.hoffmann@tue.nl
[2] University of Duisburg-Essen, Schützenbahn 70, D-45117 Essen, Germany
[3] Dutch Polymer Institute, P.O. Box 902, 5600 AX Eindhoven, The Netherlands
E-mail: j.loos@tue.nl

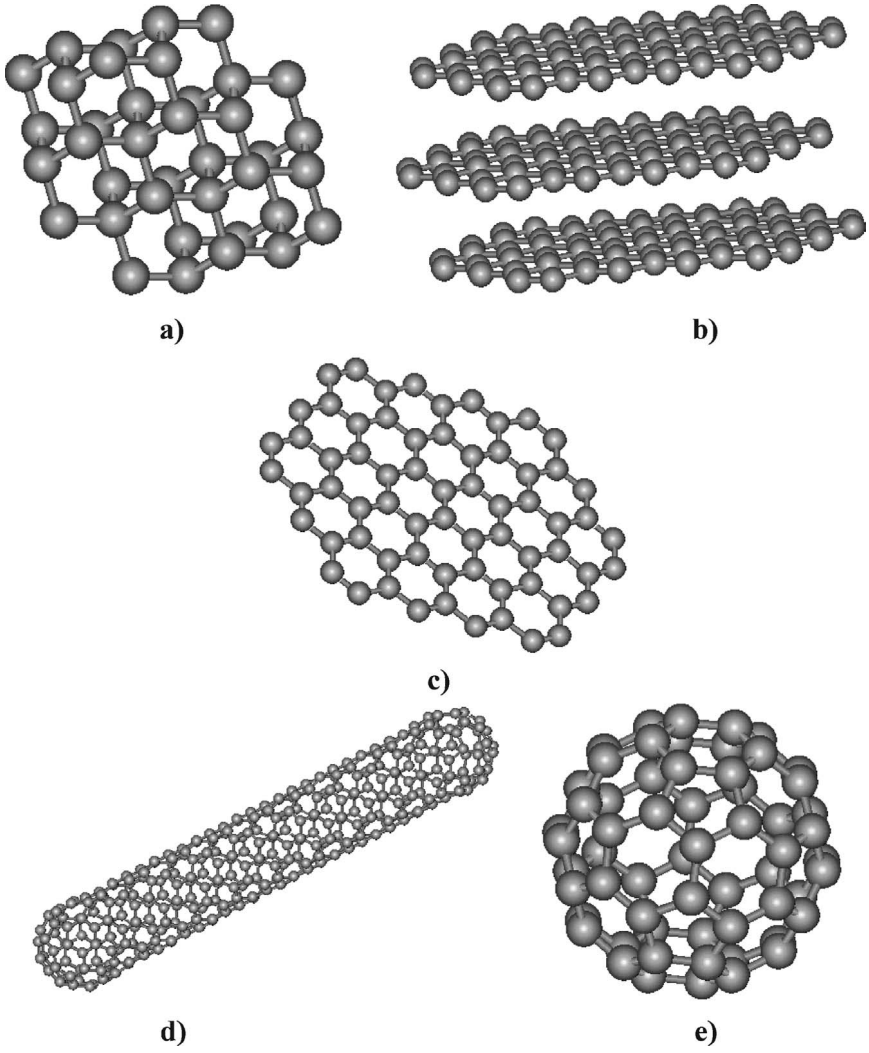

Figure 1.
(a) Diamond lattice and (b) graphite, both three-dimensional structures, (c) graphene (two-dimensional), d) single wall carbon nanotube (one-dimensional), and (e) Buckminsterfullerene (zero-dimensional).

well as inorganic materials like Si) with nanometer resolution, merely depending on probe quality. Only recently TERS imaging was demonstrated with lateral resolution far better than 50 nm and made it possible to identify local defects along one individual single wall carbon nanotube. The group of Novotny and Hartschuh[9–13] realized a resolution of 15 nm while reaching an enhancement of 4, whereas our group resolved about 30 nm while enhancing the G^+-line 256 times.[14]

The potential of TERS is enormous: TERS on biological macromolecules such as proteins and ribonucleic acid (RNA) as well as on various organic dyes has been demonstrated and resulted in spectra that are enhanced compared to conventional confocal Raman spectroscopy by factors 10^6 to 10^{14}, as claimed by the authors; on the other hand, from theoretical considerations even sub-nanometer spatial resolution, resolution below the curvature size of the actual SPM tip, should be possible to be

realised by tuning the interaction between tip and sample.

It is the purpose of our study to introduce recent results obtained on various carbon allotropes by micro-Raman spectroscopy and TERS. Main focus is to demonstrate that all carbon allotropes show variations in their Raman characteristics, which allows us, ultimately, to locally identify lateral variations of the composition or defects in carbon-based materials with nanometer resolution by means of TERS.

Experimental Part

A general view of the multi-purpose scanning near-field optical spectrometer NTEGRA SPECTRA^{TM} (NT-MDT) is shown in Figure 2. This back-scattered geometry based configuration for analysing a specimen on transparent substrates allows us to record: atomic force or shear force microscopy (AFM/SFM) images (topography, phase contrast, etc.), confocal optical images, confocal far-field Raman and fluorescence spectra and images, tip-enhanced near-field Raman spectra and images (fluorescence enhancement/quenching). A cw linearly-polarized laser beam from a He-Ne laser operating at 632.8 nm ($E = 1.96$ eV, TEM_{00}) enters the spectrometer through a single-mode optical fibre. The laser output passing through the plasma line filter is expanded and converted to a mode with a given polarization (linear, circular, radial, azimuthal). After that it is reflected by the edge-filter and goes into the inverted optical microscope (Olympus IX70) through an unpolarised beam-splitter cube (10/90) and a pinhole. A 100x oil immersion objective

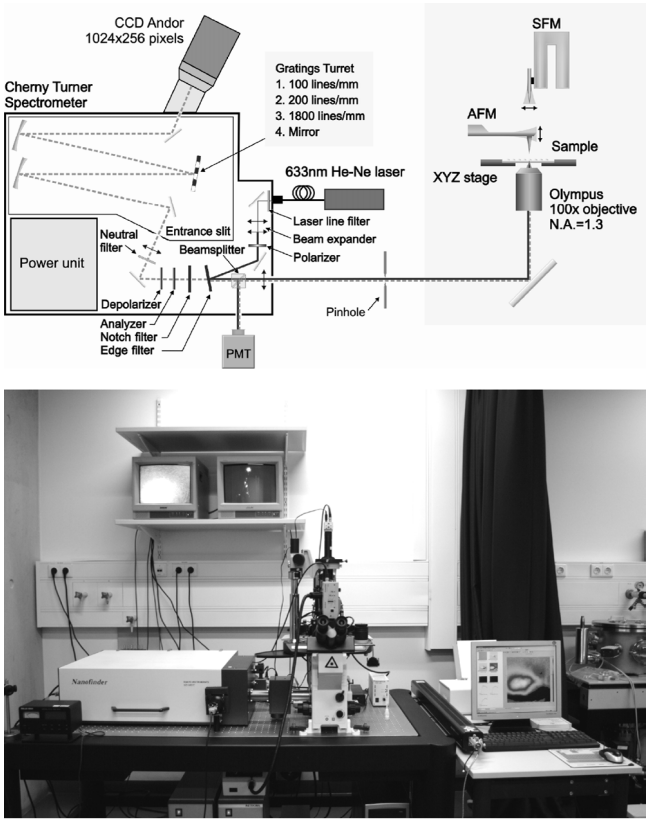

Figure 2.
(top) Optical setup of the TERS instrument used, and (bottom) photography of the TERS setup.

(Olympus, n.a.=1.3, refractive index of oil $n = 1.516$) focuses the laser beam into a spot with a size of less than 300 nm and the power at sample is about 100 μW. The tip is positioned into one of two longitudinal lobes near rims of the diffraction-limited laser spot to locally enhance the electromagnetic field beneath its apex. This system allows one to lock the tip position inside the laser spot to maintain optimum illumination conditions. A near-field Raman image is established by raster scanning the sample with a *xy*-scan stage equipped with a close-loop operation system. Scattered and/or reflected light is collected with the same objective and directed back to the spectrometer through the pinhole. An additional Kaiser notch-filter is installed into the optical path to suppress the Rayleigh scattering. In the laser confocal and spectral modes the light transmitted by the beam-splitter cube is detected with a photomultiplier (Hamamatsu, PMT943-02) and a thermoelectrically cooled charge-coupled detector (ANDOR, DV420), respectively. All Raman spectra were recorded within a spectral range of 150–2500 cm^{-1}. A 200 lines/mm grating provides a spectral resolution of better than 15 cm^{-1}. The pinhole size was equal to 40 μm because of making use of the 100x oil immersion objective.

Sample Preparation

We utilized purified single wall carbon nanotubes (SWCNTs, HiPCo, Carbon Nanotechnology Inc.) as a proper one-dimensional object with strong Raman active spectral lines for testing ultrahigh spatial resolution. A dispersion was prepared by mixing 0.05 g SWCNTs with 20 g dichloromethane in a flask and then sonicating the resulting dispersion for about 1 hour. The sonication was carried out using a horn sonicator (Sonic Vibracell VC750) with a cylindrical tip (10 mm end cap in diameter). The output power was 20 W and, therefore, delivering energy was 1100–1200 J/min. The flask was placed inside a bath with ice water during sonication in order to prevent rising of the temperature. A droplet of this dispersion was spin coated at 300 rpm for 2 min on a microscopy cover glass slide. The glass slide was preliminarily cleaned in a ''piranha'' solution (H_2SO_4:H_2O_2) at ambient conditions for 30 min, then rinsed in CH_3OH and finally dried under a continuous N_2-gas flow. A similar procedure was applied for preparation of graphene sheets but starting from highly oriented pyrolytic graphite (HOPG, NT-MDT), and for the C_{60} material (Aldrich).

Transmission electron microscopy (TEM) investigation of graphene after dispersing in aqueous solutions were performed using a Tecnai 20 (FEI Co.) operated at 200 kV. The samples were prepared by dipping a copper TEM grid in the graphene dispersion and subsequent drying.

Results and Discussion

Diamond and Amorphous Carbon

The Raman spectrum of diamond has been reported to consist of a single sharp line at 1332 cm^{-1} (e.g. Knight and White[15] and Figure 3). On the other hand, glassy carbon is a material composed of varying amounts of graphite and amorphous carbon. Two broad lines are observed at 1340 and 1590 cm^{-1}. These results are consistent with the turbostratic structure, which has been suggested for glassy carbon (with a particle size L_a of approximately 30 Å) by Nathan *et al.*[16] The corresponding spectrum is shown in Figure 3. Diamond layers deposited by vapour deposition (CVD) find a growing number of applications e.g. in electronics technology due to their hardness, insulating properties and thermal conductivity while being transparent to broad ranges of UV, visible and infrared radiation.[5] In these layers small diamond crystallites are surrounded by graphite and amorphous carbon in the grain boundaries. Raman spectroscopy e.g. is applied to easily discriminate these non-diamondoid impurities by their variations of the Raman spectrum, and thus it is employed to judge the quality of such coatings.

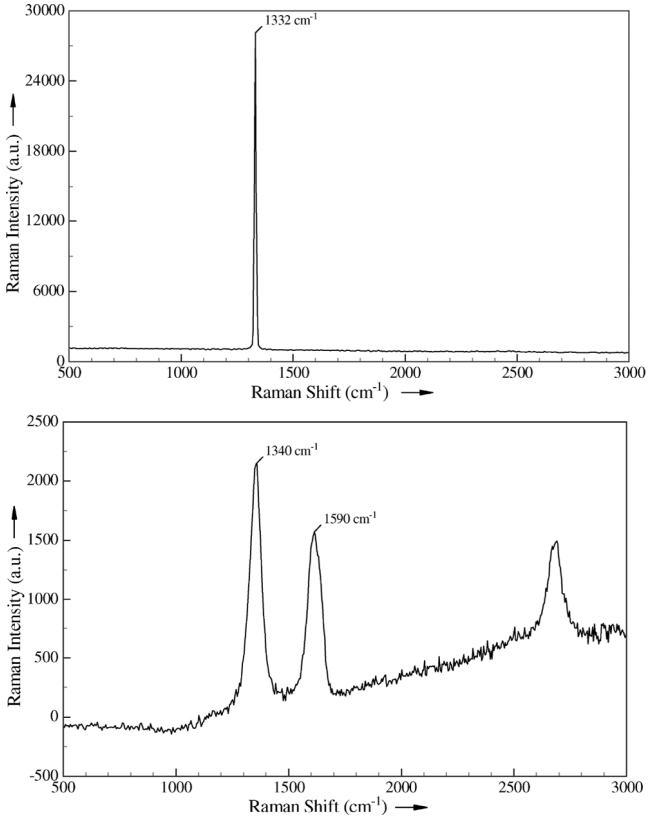

Figure 3.
(top) Micro-Raman spectroscopy spectra of a gem-quality (*tw, vsi*) diamond, and (bottom) glassy carbon.

Graphite

Another example on how Raman spectroscopy can distinguish between crystalline and amorphous order of carbon is presented by analyzing graphite. In single crystalline graphite Tuinstra and Koenig[17] only found a single line at 1575 cm^{-1} (Figure 4). This is called the G-peak (from graphite). Analysing highly ordered pyrolytic graphite (HOPG) by micro-Raman spectroscopy we can confirm the presence of this band and only this band, which suggests that the sample has very high crystallinity. In graphite of lower quality, however, one also encounters a Raman band at 1355 cm^{-1}, called D-line (from disordered graphite, Figure 4b). The ratio G-band versus D-band Raman intensity tells us about the ordered/disordered state of graphite, and thus e.g. about its conductivity.

C_{60} Buckminsterfullerene

Looking with Raman spectroscopy to Buckminsterfullerenes (C_{60} molecules), on the other hand, results in more complex Raman spectra than for diamond, amorphous carbon or graphite. C_{60} molecules are produced together with C_{70} according to the method of Krätschmer *et al.*[18] by heating graphite in an inert gas. From the soot produced the pure compound can be separated by liquid chromatography on silica. Due to the high symmetry of the molecule, the infrared spectrum shows only four lines. The Raman spectrum, as it is complementary to the IR spectrum, shows much more lines, and if, measured with excitation by visible light, is complicated by the fact that a resonance Raman spectrum is produced. Bethune *et al.*[19] measured the Raman spectrum of C_{60} with an argon ion laser and reported a line at 1470 cm^{-1} as the strongest,

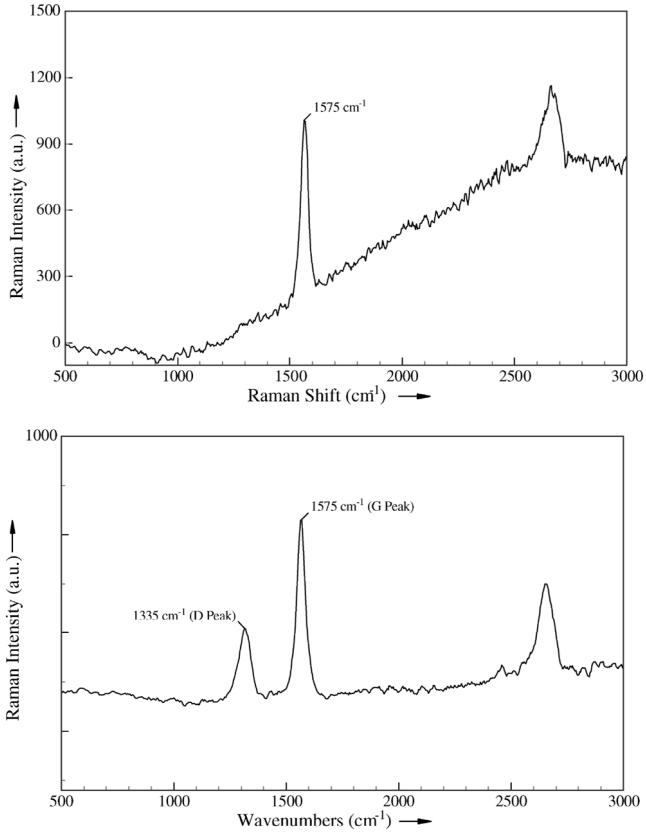

Figure 4.
Micro-Raman spectra of (top) highly ordered pyrolytic graphite, and (bottom) conventional graphite.

which corresponds well with our own measurements (Figure 5). Neugebauer *et al.*[20] calculated the Raman and IR vibrational spectrum of Buckminsterfullerenes on a high theoretical level, but without taking into account resonance effects. The visible lines in our experimental spectrum match the calculated ones in frequency but not in intensity, as

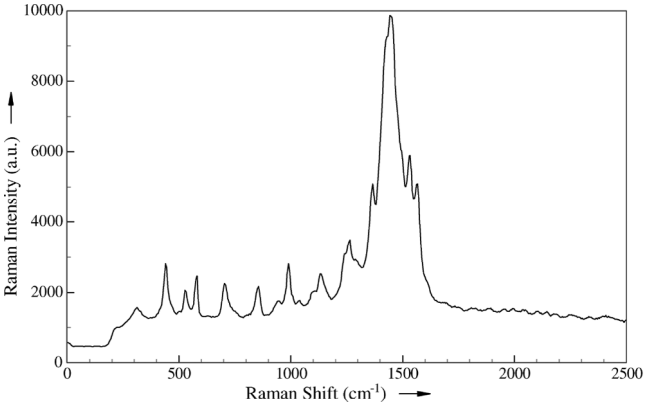

Figure 5.
Micro-Raman spectrum of a Buckminsterfullerene (C_{60}) film obtained with a laser source with wavelength of 633 nm.

our tip-enhanced Raman spectrum actually is a resonance Raman spectrum.

Single Wall Carbon Nanotubes

Single wall carbon nanotubes (SWCNTs) can be grown from the vapour phase at higher temperatures using transition metal catalysts. Formally one can build these tubes by rolling a single graphene sheet and connecting the edge carbon atoms. Similar to graphite, the Raman spectrum of SWCNTs shows as main lines the D-line at 1390 cm^{-1}, and the G^+-line 1594 cm^{-1}, slightly shifted when comparing with graphite, and an additional Raman band, the radial breathing mode (RBM) at 290 cm^{-1}, which can be used to calculate the diameter of the tubes. The ratio of D to G^+-line can be used advantageously in scans of SWCNTs to detect defects in the otherwise perfect periodically arranged atoms of the tube.[13] For the conventional Raman spectroscopy setup, a large quantity of SWCNTs are analysed at the same time and the average amount and type of defects can

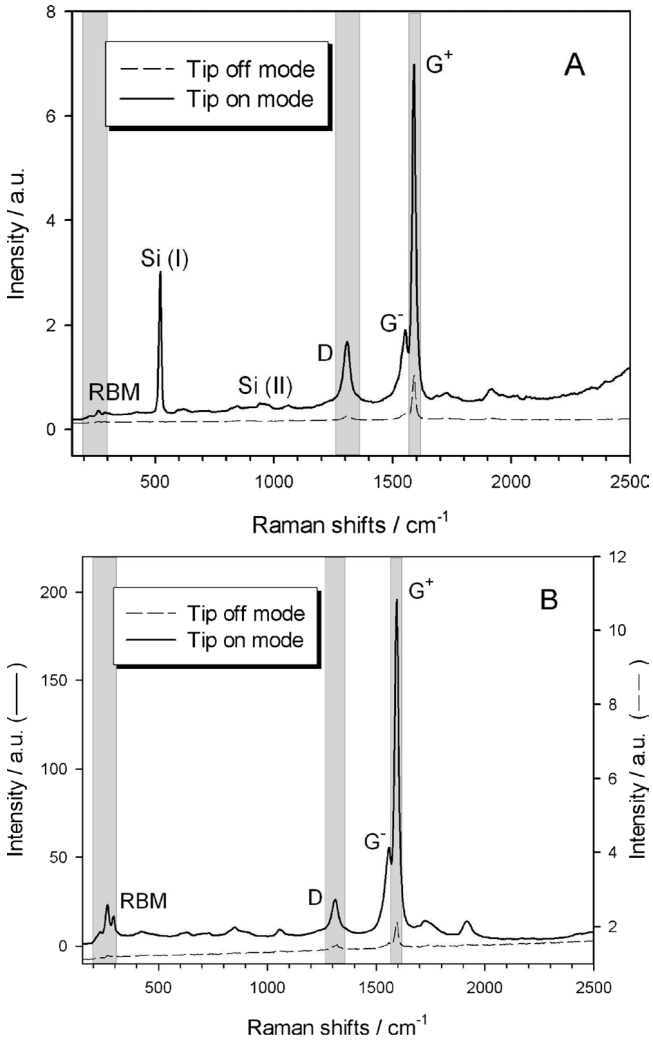

Figure 6.

Tip-enhanced Raman spectra of carbon nanotube bundles, (top) taken with a gold-coated AFM tip and (bottom) a self-made gold SFM tip. Note the much larger enhancement of the gold SFM tip (from Ref. 14).

be calculated, however, e.g. to learn more about local defect distribution at individual SWCNT to optimise procedures for functionalisation of SWCNTs, recently TERS was introduced.

Based on the concept of evanescent waves existing in the near-field (<100 nm) optical measurements beyond the diffraction limit are possible for attaining ultra-high resolution in optical spectroscopy. A practical implementation of that has become possible by combining optical spectroscopy and scanning probe microscopy (SPM), often referred to as apertureless near-field optical microscopy, and in particular, TERS. The crucial role in TERS is played by the SPM tip as a nanoscopic scatterer and/or lighting source. In the first case, the tip disturbs a confined non-radiating electromagnetic field in the proximity of a nanometer-sized specimen and converts it to a radiating one, which can be then detected by standard diffraction-limited optics. In the second case, a tip localises and enhances the scattered optical radiation over the incident one due to the coupled excitation of free electrons and the electromagnetic field present (called localised surface plasmon) in the metal of the tip. The latter is caused by the fact that namely metals, due to their small skin effect, provide the highest enhancement and scattering efficiency. An additional contribution to the field enhancement,

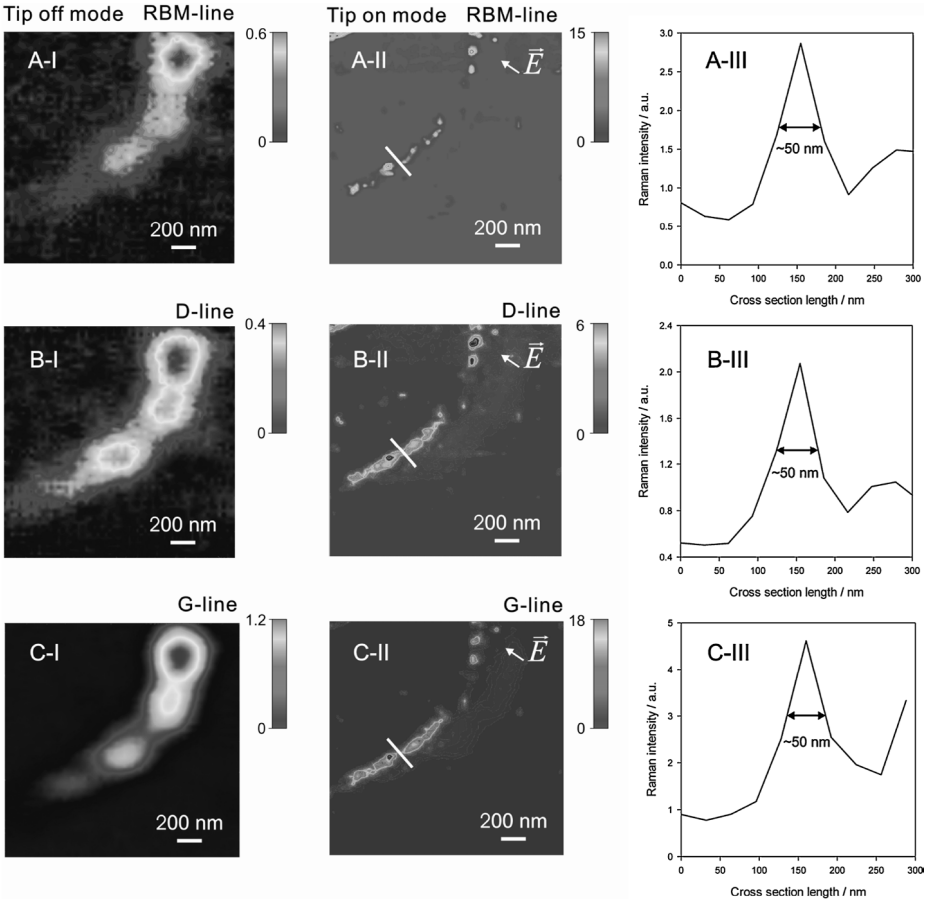

Figure 7.
Confocal (left) and tip-enhanced Raman (middle) scans on carbon nanotubes, using the radial breathing mode (RBM) line as well as the D- and G^+-lines. The cross sections indicated as a white bar in the middle scans are shown on the right (from Ref. 14).

known as quasi-static lighting rod effect, comes from a purely geometrical factor of the tip resulting in a quasi-singularity of the electromagnetic field near its apex. The material composition of the tip, its geometry and the polarization state of the incident light in the local excitation-based scheme are of the greatest importance for efficient enhancements.

Figure 6 shows tip-enhanced Raman spectra of SWCNT bundles that were taken with a gold-coated AFM tip as with a self-made gold SFM tip for tip-off (SPM tip is far away from the sample surface) and tip-on operation mode (tip is close to the sample surface and active in the nearfield). The gold SFM tip shows a much larger enhancement than the gold-coated AFM tip (256 compared to 9 for the G-line, linear enhancement, not area corrected). More details on the experiments performed can be found in reference.[14]

As the next step towards achievement of local Raman data by TERS is spectroscopic imaging. We have compared confocal and tip-enhanced Raman topographical scans on SWCNTs (Figure 7), using the radial-breathing mode (RBM) line as well as the D- and G^+-lines. Cross sections from these scans indicate a resolution of at least 50 nm (original data, 30 nm from a Gaussian fit) for the TERS scan, compared to approximately 300 nm for the confocal scan. These results demonstrate the potential of TERS imaging for local nanometer scale spectroscopic analysis of functional materials.

Graphene

Finally, we would like to introduce first TERS data obtained on graphene. It has

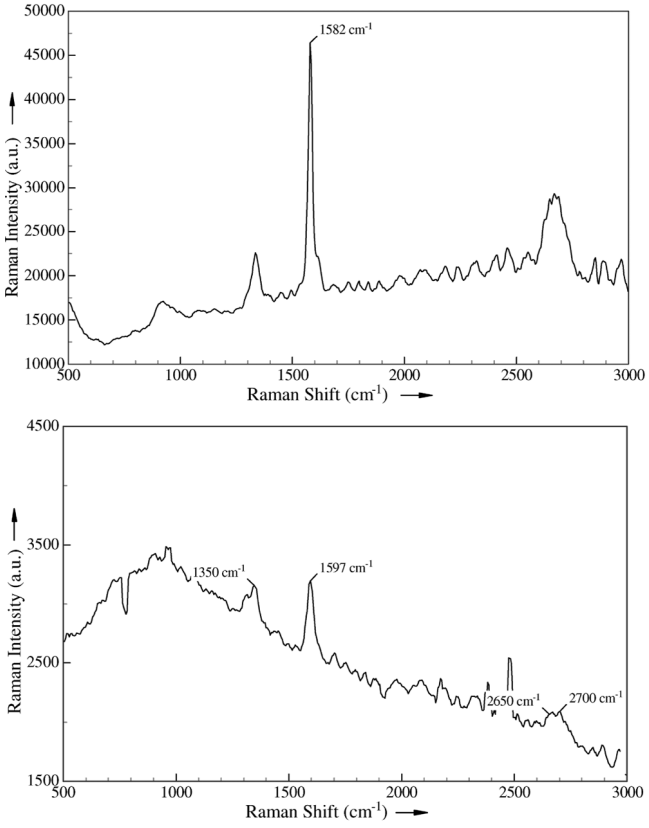

Figure 8.
Micro-Raman spectrum of (top) impure bulk grapheme, and (bottom) tip-enhanced Raman spectrum of impure graphene sheets.

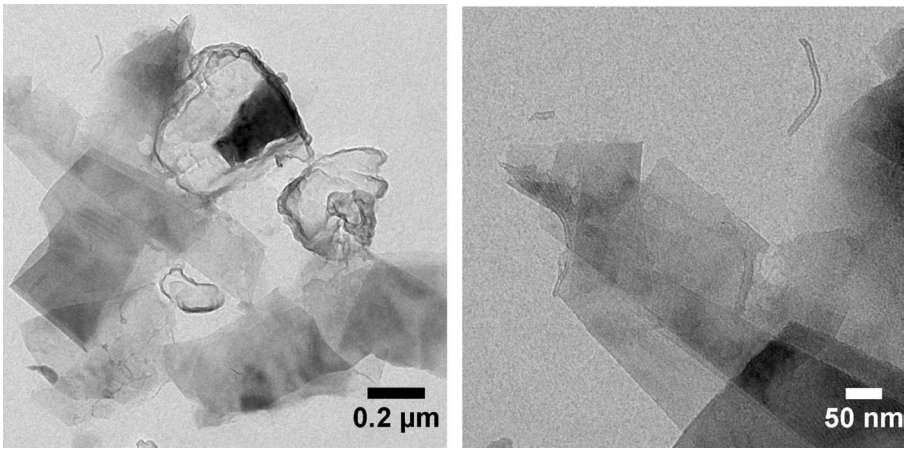

Figure 9.
TEM images of representative graphene samples.

been first described by Novoselov *et al.*[3] as monocrystalline graphitic films, which are a few atoms thick but are nonetheless stable under ambient conditions, metallic, and of remarkably high quality. The films were found by the authors to be a two-dimensional semimetal with a tiny overlap between valence and conductance bands. The conventional Raman spectrum of graphene and graphene layers has been studied in great detail by Ferrari *et al.*[21]. Graphene shows a Raman spectrum very similar to that of graphite, the differences observed mirror the missing interaction between the layers. The D peak second order changes in shape, width, and position for an increasing number of layers, reflecting the change in the electron bands via a double resonant Raman process, and the G peak slightly down-shifts.

We report here the first measured TERS spectrum of graphene. The graphene used by us has been prepared from HOPG and is still containing graphite flakes. These and the edges of the graphene flakes can be detected in the graphene bulk spectrum by the line at 1350 cm^{-1} (Figure 8). A representative transmission electron microscopy (TEM) image of a similar sample is shown in Figure 9, which shows single as well as stacked layers of graphene. The spectrum was taken from a part of the sample (graphene and flakes) where no material was detected optically indicating only very little amount of material was present. The TERS spectrum suggests that the area under inspection was at the edge of graphene flakes, as the band at 2700 cm^{-1} shows a split structure of approximately equal height, while pure graphene would only produce a single line (that at 2650 cm^{-1}). The band at 2700 cm^{-1} in the graphite Raman spectrum at higher resolution has a shoulder at lower wavenumbers, it is the second order of zone-boundary phonons, the results presented are only preliminary data and our study of graphene still is in progress.

Conclusion

Applying Raman spectroscopy helps understanding better the organisation of various carbon allotropes. Raman spectra of diamond, amorphous carbon, graphite, single wall carbon nanotubes (SWCNTs) and graphene sheets show different bands and band positions dependent on the degree of crystallinity, perfectness of their organisation or number of defects of the material under investigation. These variations can be used to determine the quality of the carbon-based materials, e.g. by comparing the intensities of the G^{+}- and D-bands. Ultimately, Raman spectroscopy combined with a scanning probe microscopy setup,

so-called apertureless near-field optical microscopy, and in particular tip-enhanced Raman spectroscopy and imaging, allows detection of such defects with lateral resolution in the nanometer range. We have demonstrated TERS on SWCNT and graphene samples, and in both cases high enhancement factors are obtained. In case of SWCNT, TERS imaging with lateral resolution far better than 50 nm is obtained and the results obtained reflect the local heterogeneity of individual SWCNTs on the nanometer length scale. Currently, similar investigations on graphene samples are in progress

Acknowledgements: The authors are grateful to Dr. J. Yu (Donghua University, Shanghai, China), Ing. S. van Bavel, and Dr. K. Lu for their help in preparing samples, to Dr. S. S Kharintsev and Dr. A. Kodentsov for carbon and graphite samples and stimulating discussions. The authors also acknowledge technical assistance from Dr. P. Dorozhkin and Dr. I. Dushkin (NT-MDT, Russia). This research has been supported by the Ministry of Economic Affairs of the Netherlands via the Technologische Samenwerkings project QUANAP (SenterNovem TSGE3108).

[1] H. Kroto, J. R. Heath, S. C. O'Brian, R. F. Curl, R. E. Smalley, *Nature* **1985**, *318*, 162.
[2] S. Iijima, *Nature* **1991**, *354*, 56.
[3] K. S. Novoselov, A. K. Geim, S. V. Morozov, D. Jiang, Y. Zhang, S. V. Dubonos, I. V. Grigorieva, A. A. Firsov, *Science* **2004**, *306*, 666.
[4] K. I. Katsnelson, *Materials today* **2007**, *10*, 20.
[5] J. Filik, *Spectroscopy Europe* **2005**, *17*, 10.
[6] I. R. Lewis, P. R. Griffith, *Appl. Spectrosc.* **1996**, *50*, 12A.
[7] R. K. Chang, "*Surface Enhanced Raman Scattering*", T. E. Furtak, Eds., Plenum Press, New York **1982**.
[8] Y. Inue, S. Kawata, *Opt. Lett.* **1994**, *19*, 159.
[9] L. Novotny, E. J. Sanchez, X. S. Xie, *Ultramicroscopy* **1998**, *71*, 21.
[10] E. J. Sanchez, L. Novotny, X. S. Xie, *Phys. Rev. Lett.* **1999**, *82*, 4014.
[11] A. Hartschuh, E. J. Sanchez, X. S. Xie XS, L. Novotny, *Phys. Rev. Lett.* **2003**, *90*, 095503.
[12] L. Novotny, S. J. Stranick, *Annu. Rev. Phys. Chem.* **2006**, *57*, 303.
[13] N. Anderson, A. Hartschuh, S. Cronin, L. Novotny, *J. Am. Chem. Soc.* **2005**, *127*, 2533.
[14] S. S. Kharintsev, G. G. Hoffmann, P. S. Dorozhkin, G. de With, J. Loos, *Nanotechnology* **2007**, *18*, 315502.
[15] D. S. Knight, W. B. White, *J. Mater. Res.* **1990**, *5*, 385.
[16] M. I. Nathan, J. E. Smith, Jr., K. N. Tu, *Journal of Applied Physics* **1974**, *45*, 2370.
[17] F. Tuinstra, J. L. Koenig, *J. Chem Phys.* **1970**, *53*, 1126.
[18] W. Krätschmer, K. Fostiropoulos, D. R. Huffman, *Chem. Phys. Lett.* **1990**, *170*, 167.
[19] D. S. Bethune, G. Meijer, W. C. Tang, H. J. Rosen, W. G. Golden, H. Seki, C. A. Brown, M. S. de Vries, *Chem. Phys. Lett.* **1991**, *179*, 181.
[20] J. Neugebauer, M. Reiher, C. Kind, B. A. Heß, *J. Comp. Chem.* **2002**, *23*, 895.
[21] A. C. Ferrari, J. C. Meyer, V. Scardaci, C. Casiraghi, M. Lazzeri, F. Mauri, S. Piscanec, D. Jiang, K. S. Novoselov, S. Roth, A. K. Geim, *Phys. Rev. Lett.* **2006**, *97*, 187401.

 DOI: 10.1002/masy.200850502

Broadband Dielectric Relaxation Spectroscopy in Polymer Nanocomposites

Polycarpos Pissis,[*1] *Daniel Fragiadakis,*[1] *Athanasios Kanapitsas,*[2] *Kostas Delides*[3]

Summary: Dielectric spectroscopy in the frequency domain and thermally stimulated depolarization currents techniques, covering together a broad frequency range (10^{-4} – 10^{9} Hz), were employed to investigate molecular dynamics in relation to structure and morphology in polymeric nanocomposites. Several systems were investigated, three of them with the same epoxy resin matrix and different inclusions (modified smectite clay, conducting carbon nanoparticles and diamond nanoparticles) and two with silica nanofiller (styrene-butadiene rubber/silica and polyimide/silica nanocomposites). Special attention was paid to the investigation of segmental dynamics associated with the glass transition of the polymer matrix, in combination also with differential scanning calorimetry measurements. Effects of nanoparticles on local (secondary) relaxations and on the overall dielectric behavior were, however, also investigated. Several interesting results were obtained and discussed for each of the particular systems. Two opposite effects seem to be common to the nanocomposites studied and dominate their behavior: (1) immobilization/reduction of mobility of a fraction of the chains at the interface to the inorganic nanoparticles, due to chemical or physical bonds with the particles, and (2) loosened molecular packing of the chains, due to tethering and geometrical confinement, resulting in an increase of free volume and of molecular mobility.

Keywords: dielectric spectroscopy; glass transition; polymer nanocomposites; segmental dynamics

Introduction

The mechanical and the physical properties of polymer nanocomposites, i.e. composite materials with a polymeric matrix and, typically, inorganic fillers with characteristic size in the range of 1–100 nm, are often significantly improved, as compared to those of the polymer matrix, for much smaller filler content than would be required for conventional macroscale or microscale composites.[1,2] Polymer nanocomposites also exhibit distinctive properties related to the small particle size and correspondingly small mean interparticle spacing (typically also in the nanometer range).[3]

There is yet no satisfactory theoretical explanation for the origin of improvement of the properties of polymer nanocomposites. It is generally accepted, however, that the large surface to volume ratio of the nanoscale inclusions plays a significant role. Results obtained by various experimental techniques, as well as by theory and computer simulations, indicate the presence of an interfacial polymer layer around the filler, with structure/morphology and chain dynamics modified with respect to the bulk polymer matrix.[4–9] The existence of such an interfacial layer has been postulated for conventional composites long ago and various experiments provided

[1] National Technical University of Athens, Department of Physics, Zografou Campus, 157 80 Athens, Greece
E-mail: ppissis@central.ntua.gr
[2] Technological Education Institute (TEI) of Lamia, Department of Electronics, 35100 Lamia, Greece
[3] Technological Education Institute (TEI) of West Macedonia, Laboratories of Physics and Materials Technology, Kozani, Greece

support for that.[10,11] Questions related to the existence of such an interfacial layer, its thickness and the variation of polymer properties within the layer with respect to bulk properties become crucial for nanocomposites. The reason for that is that, due to the small particle size, resulting in a large surface area presented to the polymer by the nanoparticles, the interfacial layer can represent a significant volume fraction of the polymer in nanocomposites.[3]

Broadband dielectric relaxation spectroscopy (DRS) has proved to be a powerful tool for investigation of molecular dynamics of polymers and composites.[12,13] The main advantage of DRS, as compared to other similar techniques for studying molecular dynamics, is the broad frequency range, which can be relatively easily covered[13] (10^{-4}–10^{9} Hz in the present work). This broad frequency range allows to measure on the same sample processes with very different characteristic (relaxation) times and, correspondingly, different characteristic length scales.

Guided by theory and by results obtained with model systems of geometrical confinement, we have investigated over the last few years molecular dynamics in nanostructured polymers and in polymer nanocomposites with various matrices and fillers. To that aim we employed ac dielectric spectroscopy in the frequency domain and, to a lesser extent, a second dielectric technique in the temperature domain, thermally stimulated depolarization currents – TSDC, differential scanning calorimetry (DSC) and dynamic mechanical analysis (DMA). Here we present and discuss comparatively to each other results obtained with five selected nanocomposite systems, three of them with the same epoxy resin matrix and different inclusions (modified smectite clay, conducting carbon nanoparticles and diamond nanoparticles) and two with silica nanofiller (styrene-butadiene rubber/silica and polyimide/silica nanocomposites). The preparation of the nanocomposites, the morphological characterization and details of the dynamics studies have been presented/will be presented for each particular system elsewhere. In this comparative study we focus on common features and differences in the effects of nanoparticles on the polymer matrix dynamics, as revealed by dielectric techniques. Effects on the overall dielectric behavior, on local (secondary) relaxations and, in particular, on segmental dynamics, associated with the glass transition (dynamic glass transition), are critically discussed.

Experimental Part

Details of the preparation and characterization of the materials have been given elsewhere.[14–17] The nanocomposites investigated include: (1) epoxy resin/modified smectite clay (ER/clay) nanocomposites of exfoliated structure[14]; (2) epoxy resin/nanosized carbon particle (ER/NCP) nanocomposites with a mean particle diameter of about 10 nm[15]; (3) epoxy resin/diamond (ER/diamond) nanocomposites with a mean particle diameter of about 6 nm[16]; (4) styrene-butadiene rubber/silica (SBR/silica) nanocomposites[6]; (5) polyimide-silica (PI/silica) nanocomposites prepared by sol-gel techniques.[17]

For ac dielectric spectroscopy measurements the complex dielectric function, $\varepsilon = \varepsilon' - i\varepsilon''$, was determined as a function of frequency and temperature.[12,13] In addition to ac dielectric spectroscopy measurements, the non-isothermal dielectric technique of thermally stimulated depolarization currents (TSDC) was used. TSDC consists of measuring the thermally activated release of frozen-in polarization and corresponds to measuring dielectric losses as a function of temperature at low equivalent frequencies of 10^{-2}–10^{-4} Hz.[18] Details of the measurements and of the various formalisms used for the presentation and analysis of the data have been given elsewhere.[14–17]

Results and Discussion

Overall Dielectric Behavior

Figure 1 shows results obtained with SBR/silica nanocomposites.[6] The composition

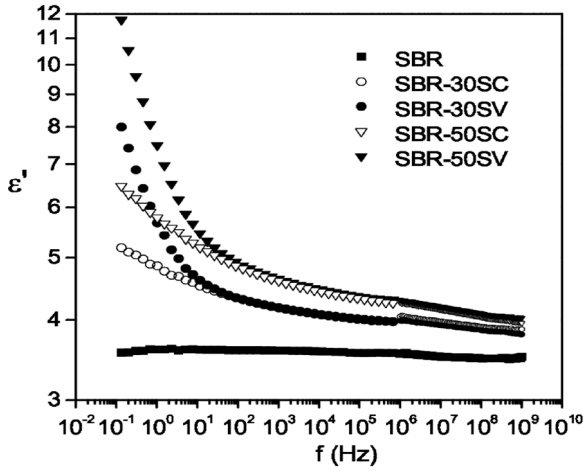

Figure 1.
Real part of dielectric function ε' against frequency f at 25 °C for the SBR/silica nanocomposites indicated on the plot.

of SBR was 23.5 wt% styrene and 76.5 wt% butadiene. The filler used (30 and 50 wt%, nominal) was a precipitated amorphous silica, non-treated (code SV) and pre-treated (code SC) to render the surface organophilic.[6] The results show that ε' increases with increasing amount of filler. This can be understood in terms of a higher dielectric constant of the filler than the matrix and effective medium formulae[17] and/or increased molecular mobility of the polymeric chains. The values of ε' in the nanocomposites of Figure 1 exceed, however, those of pure silica ($\varepsilon' = 3.8$–4.0 at 25 °C[17]), indicating that the data can not be explained solely on the basis of mixture formulae. The hypothesis of increased molecular mobility of the polymeric chains resulting from increase of free volume due to loosened molecular packing of the chains confined between the nanoparticles[19] will be further discussed later on the basis of results for the dielectric strength (magnitude) of secondary and primary relaxations.

A dielectric relaxation is observed in Figure 1 (step in ε'(f)) centered at 10^6–10^7 Hz. This is the segmental α relaxation associated with the glass transition of SBR to be studied in more detail in the next section. The increase in ε'(f) with decreasing frequency for $f \leq 10^3$ Hz, not observed in the pure matrix, originates from space charge polarization and dc conductivity effects. The results in Figure 1 show that these effects are more pronounced in the samples with non-treated silica particles, whereas dipolar effects at higher frequencies do not depend on filler treatment. It is reasonable to assume that space charge polarization originates from the accumulation of charges in the volume of polymer trapped within agglomerates formed by the nanoparticles. The higher values of space charge polarization in the composites with non-treated filler suggest then that the degree of agglomeration is larger in these composites. These results suggest that low-frequency ac measurements are sensitive to changes in the morphology, in agreement with results for the glass transition and the α relaxation by DRS and DSC (this work) and by DMA.[6]

Figure 2 shows TSDC and Figure 3 ac results for the ER/NCP nanocomposites. The data in Figure 3 have been recorded isothermally by scanning the frequency and have been replotted here. A relatively high frequency has been chosen for the presentation, in order to eliminate conductivity effects present at lower frequencies. An

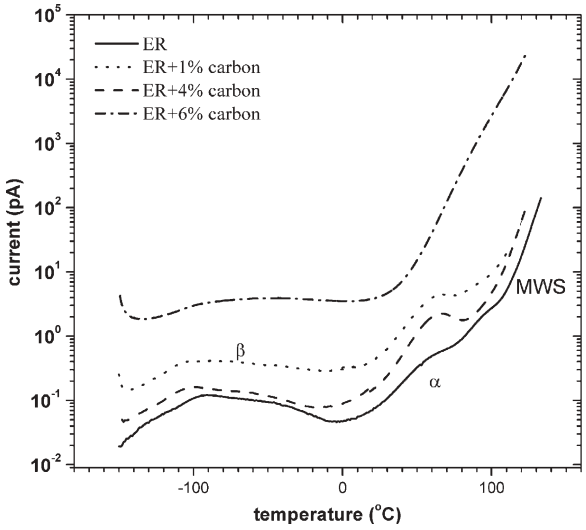

Figure 2.
TSDC thermograms for the ER/carbon nanocomposites indicated on the plot.

overall increase of molecular mobility is observed in Figure 3, in agreement with TSDC data for the same samples shown in Figure 2, in the sense that, at each temperature, ε' and ε'' increase with increasing filler content. This is to a large extent related to the formation of a percolation structure of the nanoparticles, as confirmed by the dependence of ε' (at a frequency of 1Hz and a temperature of $-50\,^{\circ}C$) on volume concentration p of NCP in the inset to Figure 3(a). The well-known equation for the dependence of ε' on p from percolation theory.[20]

$$\varepsilon'(p) = \varepsilon'_m + A|p - p_c|^{-t} \quad (1)$$

where m refers to the matrix, p_c is the percolation threshold and t the critical exponent, has been fitted to the data and the values of p_c and t determined to 7.4% and 0.69 respectively. Two relaxations, a secondary β relaxation at lower temperatures and the segmental α relaxation at

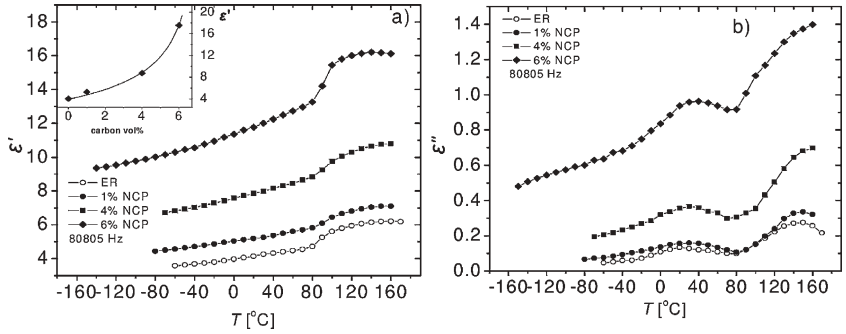

Figure 3.
Temperature dependence of the real ε' (a) and the imaginary part ε'' (b) of the dielectric function of the samples indicated on the plot at 80805 Hz. The inset shows ε' (measured at 1Hz and $-50\,^{\circ}C$) against volume concentration of NCP. The line is a fit of Equation (1) to the data.

higher temperatures, associated with the glass transition of the ER matrix, are observed in Figure 3. They will be studied in more detail in following sections. In the TSDC measurements on the same samples in Figure 2, in addition to the β and the α relaxations, an interfacial Maxwell-Wagner-Sillars (MWS) relaxation is observed in the ER matrix at higher temperatures (interestingly, however, not in the nanocomposites).

Figure 4 shows results obtained with PI/silica nanocomposites prepared by the in situ generation of crosslinked organosilicon nanophase through the sol-gel process.[17] The step at higher frequencies is due to the secondary γ relaxation of the PI matrix, to be discussed in the next section. The most interesting result in Figure 4 is the overall and monotonous decrease of ε' with increasing filler content. Moreover, the values are lower than those of bulk silica ($\varepsilon' = 3.8$–4.0), suggesting a looser molecular packing of PI chain fragments adjacent to the filler particles and/or a loose inner structure of the spatial aggregates of the organosilicon nanophase. By assuming a constant value of ε' for the PI matrix (the measured one, $\varepsilon'_m = 3.18$) and by using various effective medium theory formulae for the calculation of the dielectric function of a composite material[17,20] we obtained for the organosilicon nanophase ε'_i values between 2.47 and 1.58, depending on the composition and the specific formula used. The ε'_i values show, however, the same trend with composition, independently of the formula used. These results can be rationalized assuming that the organosilicon nanophase is made up of nanoparticles of silica ($\varepsilon'_m = 3.8$–4.0) fused together into loose spatial aggregates with a considerable fraction of empty inner pockets ($\varepsilon'_i = 1$). Effective medium theory calculations for this silica-air composite give for the volume fraction of air values in the range 0.40–0.65.[17]

Secondary Relaxations

The step in $\varepsilon'(f)$ in Figure 4 at frequencies higher than about 10^4 Hz is due to the local γ relaxation of the PI matrix, tentatively attributed to non-cooperative motions of the imide groups and/or adsorbed water.[17] Figure 5 shows results for the same γ relaxation in another series of PI/silica nanocomposites, prepared also by sol-gel techniques.[19] The magnitude of the relaxation increases with increasing silica content, without any change of the time scale. Similar results were obtained by TSDC measurements (also in the PI/silica nanocomposites of Fig. 4). Measurements on the same PI/silica samples at different water contents by ac

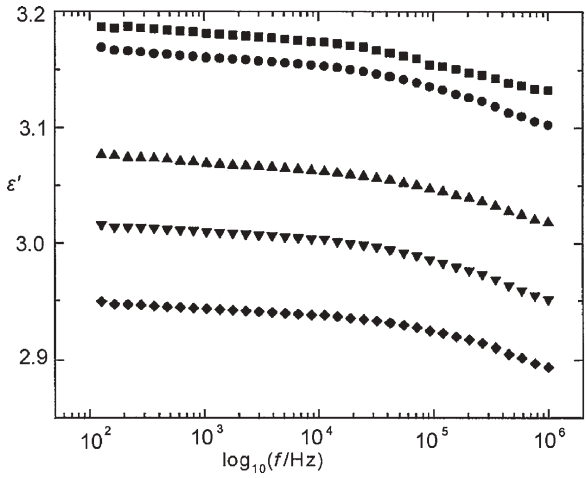

Figure 4.
Frequency dependence of the real part of the dielectric function ε' at 25 °C for PI/silica nanocomposites. The weight fraction of silica is from the uppermost to the lowermost curve 0, 8.6, 22.4, 31.7, 35.6.